ON OPTIMALITY IN HUMAN CONTROL TASKS

S.J. Merhav

Department of Aeronautical Engineering
Technion, Haifa - Israel

Abstract

Applications of optimal control theory to man-machine modelling in aircraft control indicate that experimental results of human control performance are surprisingly close to the corresponding analytical solutions for linearized models which follow from quadratic performance criteria. Recent studies have shown that this optimal-like nature of the human operator exists in widely different tasks. Two such problems are reviewed in this paper: 1) Lateral control of a low flying vehicle using visual field information. 2) Control performance using a manipulator which provides the operator with complete kinesthetic information pertaining to the controlled plant. The results contribute to improved quantitative understanding of human estimation and control functions and pave the way to improvements in the design of man-machine interfaces at the display and control levels.

1. Introduction

For more than two decades it has been recognized that mathematical models of man machine systems can be constructed for some basic control and regulating task definitions. Although the majority of successful efforts in this field have been confined to linearized models, the results have greatly contributed to the body of knowledge which underlies the design flight control systems involving human operators. The quasilinear behavior and the noisy observation and control functions of the human operator, suggested the single loop models described by Mc Ruer et al[1] (1967), where the well trained operator was modelled as a linear controller and an uncorrelated remnant noise source. The actual parameters of these models were determined by applying spectral analysis methods to the input-output data of the human operator and the results were described in terms of frequency response describing functions. The resulting models strongly indicated the adaptive nature of the human operator under varying control tasks. This suggested, already at an early stage[2], that the well trained human controller obeys certain optimization processes determined by a suitable performance criterion and the constraints imposed by the controlled plant and the physiology of the human controller. With the advent of modern control and filtering methodology and the significant progress in modelling the manual neuromotor system[3] and visual signal perception[4], the stage was set for the development of sophisticated and flexible analytical man-machine models in control and regulation tasks.[5]

The contribution of these developments to man-machine systems modelling is manifold:

1. It provides a quite general theoretical basis for predicting human operator performance in a large variety of control tasks.
2. It enables the extension of the early single loop models to multivariable and time varying systems.
3. It provides a theoretical framework within which a wide range of problems such as the efficacy of display or control augmentation or fundamentally complex display situations can be studied.

This paper addresses itself to some basic problems of vehicular control which fall within the third category mentioned above. The first problem, described in more detail in[6] is concerned with the modelling of vehicular control using basic visual field cues. This problem departs from the earlier work of Kleinman et al[5] (1971) in which the control functions derive from well defined instrument displays. The problem of vehicular control by visual field cues is of particular interest in low flying or during the landing phase in which the control functions mainly use visual field information. The understanding and the analysis of the basic structure of the control oriented information provided by the visual field, yields some fundamental guidelines for the design of display aids which can be superimposed on the visual field by head-up displays in manned aircraft or by T.V. techniques in remotely piloted vehicles.

The analytical model presented in this paper derives from the optimization of a quadratic performance criterion and the linearized equations of motion describing the lateral control of a low flying remotely piloted vehicle (R.P.V.). The analytical results (shown in greater detail in[6]) of lateral deviation, heading error and control effort are validated by laboratory experiments. The comparison between experiment and theory strongly supports the assumption that the trained operator resembles an optimal controller and that the analytical model is capable of predicting performance measures.

The second problem in this paper is concerned with the role played by kinesthetic cues in the manual control system and their potential contribution to the determination and execution of optimal control commands at the proprioceptive level. It is shown that if a manipulator is designed to provide complete kinesthetic information pertaining to the input and output of the controlled plant, as present in the direct handling of objects, the appropriate sensory organs in the neuromotor system become involved so as to provide the essential plant state estimates and the resulting optimal or near optimal control commands. This is achieved at the proprioceptive level of the nervous system while considerably unloading the estimation and decision functions usually performed in the central nervous system. A regulating task for a second order plant, involving such a manipulator, is defined in accordance with a quadratic performance criterion subject to the constraints of control effort. The analytical results, (shown in more detail in[7]) compare very well

with experiment and, again, the assumption that the human operator resembles an optimal controller is strongly supported.

The evidence presented by these examples calls for further efforts of modelling man-machine systems within an optimal control framework. In addition to the broader insights gained by this approach, it may lead to the design of better man-machine interfaces. The required loop closures given by the gain matrix of the optimal controller indicates the relative importance of displaying various state components. The capacity of the human operator's sensory organs to sense and to process and utilize this state information, determines the degree to which he is actually able to approximate the performance of an optimal controller. The examples shown in this paper demonstrate that at least for second order type systems this proximity is quite good.

2. A Model for Vehicular Control by Visual Field Cues

2.1 Background

In the visual field control (V.F.C.) task, the error by which control is accomplished is at present not clearly understood. In instrument display control the error is explicitly shown on a display, while in the V.F.C. task the error has to be derived from the visual field (V.F.). In contrast with instrument display the visual field can undergo very wide variations such as the narrowing of the field of view, range of visibility, etc. The human operator (H.O.) has the ability to adapt to these changes, although this may be at the cost of lower system performance or increased steering effort.

Mc Ruer, Weir et al. [8,9] (1968, 1969) have developed vehicular control models indicating the state variables which should be observed to obtain the required loop closures. However, it is not shown how these variables are perceived. Kleinman, Baron, Levison[5,10,11], (1970-1971) used optimal control theory for instrument display control models only. On the other hand, Gibson[12], (1950), Gordon[13], (1966), Naish[14], (1971), have developed models for the perception of visual cues. Gibson[12], as well as Gordon[13] assume that the visual field information (V.F.I.) is derived from the apparent motion of conspicuous objects in the V.F. Naish[14] assumes that the control oriented V.F.I. in the approach to landing is derived from apparent changes in runway configuration. So far these theories have not been incorporated within a control theoretic model in quantitative form.

This is attempted in this paper. The variations in the structure of the visual field expose the human controller to apparently varying control situations. However, the optimality of the well trained operator, as indicated by Kleinman et al should be maintained by his inherent adaptive properties. In the model development, the human operator's remnant noise sources, namely, observation and motor noise, are specified parametrically and then determined experimentally. In particular, observation noise, which accounts for the uncertainty in detecting the error, is strongly related to the geometry and viewing conditions of the visual field.

2.2 Formulation of the Control Error Model

Fig. 1a shows the Visual Field (V.F.) as seen from a low flying aircraft in horizontal flight and in rectilinear motion. Fig. 1b shows the corresponding plan view. According to Gibson[12] (1950), the direction of a vehicle in straight motion is indicated by a point E on the horizon, fig. 1a. Point E is the only point in the V.F. which is apparently stationary and all other textural points in the V.F. appear to have relative motion with velocity vectors (indicated by arrows) expanding from point E in straight lines, referred to as "streamers". Point E is referred to as "the focus of expansion".

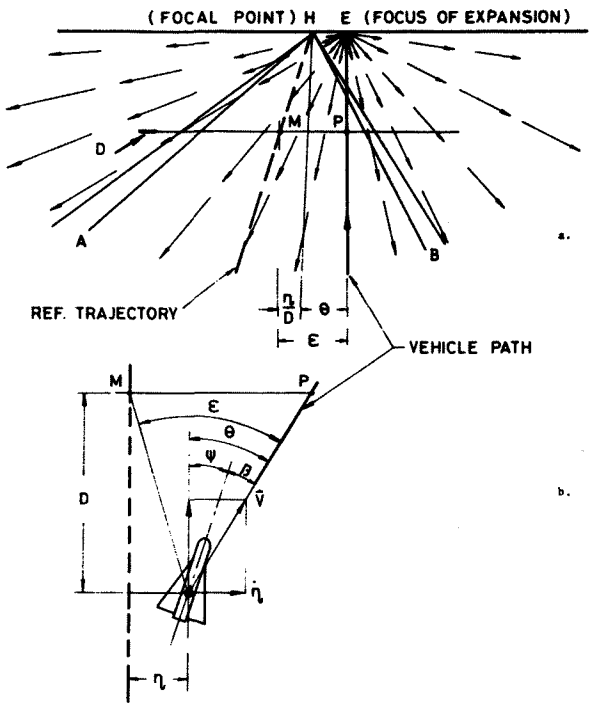

FIGURE 1. a. The Visual Field for Rectilinear Motion.
b. Plan View of Rectilinear Motion (From Ref.[6]).

In this paper a modified version of Gibson's focus of expansion[12] is adopted. Apart from point E at infinity, the direction of motion is also given by the "streamer" which appears to be vertical. This streamer is the future path of the vehicle. For curved motion shown in fig. 2a and 2b the focus of expansion no longer exists. The vehicle's future path is given by the streamer, i.e., the solid line in fig. 2a, which vertically intersects the base of the V.F. Fig. 2a shows a runway of infinite length with guidelines HA and HB and center line HX. The control task involves keeping the aircraft laterally on HX. The flight is level, at a constant height and constant speed. The notations, indicated in fig. 2b, are:

η : lateral deviation from HX
$\vec{V}$: velocity vector of the vehicle
θ : path angle, between $\vec{V}$ and HX
ψ : yaw angle, between HX and vehicle axis
β : slip angle, between $\vec{V}$ and vehicle axis.

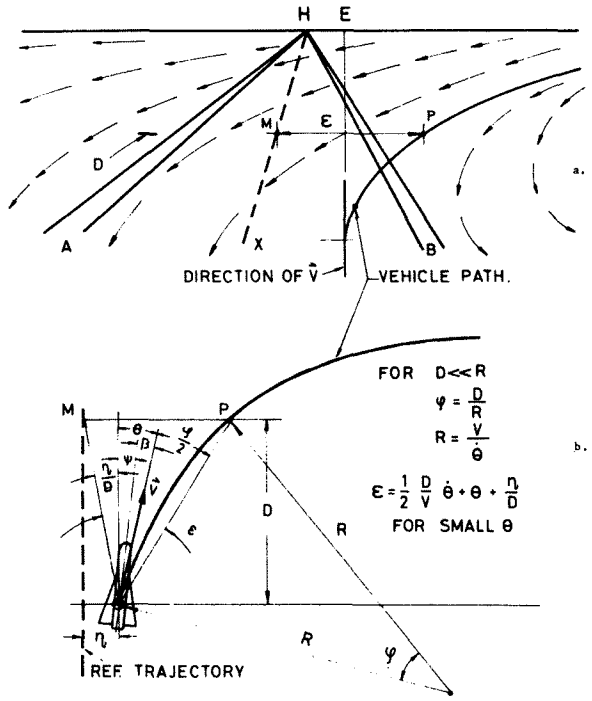

FIGURE 2. a. The Visual Field for Curved Motion.
b. Plan View of Curved Motion (From Ref.[6]).

The control error at distance D is defined in fig. 2a as the visual angle subtended between points P and M at distance D, where M is a point on HX and P a point on the future vehicle path. Following the geometry of fig. 2b, the error ε is given by:

$$\varepsilon = \frac{1}{2}\frac{D}{V}\dot{\theta} + \theta + \frac{\eta}{D} \tag{1}$$

for small θ:

$$\theta = \frac{\dot{\eta}}{V} \tag{2}$$

and (1) can be written as:

$$\varepsilon = \frac{1}{2}\frac{D}{V^2}\ddot{\eta} + \frac{\dot{\eta}}{V} + \frac{\eta}{D} \tag{3}$$

The vehicle control task involves reducing ε to zero. The V.F.I. model based on the error ε at distance D is hereafter referred to as the "single distance V.F.I. model". Since ε does only depend on the V.F. this is accomplished without vehicle based reference lines. Eq. (3) shows that the single variable ε includes information about the position as well as rate and acceleration of η. The three terms in (3) originate from:

$\frac{1}{2}\frac{D}{V^2}\ddot{\eta}$: Local inclination of streamers in the V.F.

$\frac{\dot{\eta}}{V}$: Focus of expansion or instantaneous velocity vector

$\frac{\eta}{D}$: Inclination of line HX.

It is clear that in the absence of streamers, the first term in (3) vanishes and acceleration cues are no longer perceived. In this paper the effect of streamers is disregarded and only the effect of $\vec{V}$ and the inclination of HX is considered. ε is then given by:

$$\varepsilon = \theta + \frac{\eta}{D} \tag{4}$$

with (2) and after Laplace transformation:

$$\varepsilon(s) = \frac{1}{V}\left(s + \frac{V}{D}\right)\eta(s) \tag{5}$$

(5) shows the presence of a lead zero in the feedback path. Since the vehicular dynamics is basically a double integrator, this lead zero plays an essential part in stabilizing the system, and reducing operator workload.

Remotely Piloted Vehicle (R.P.V.) control is a special case of V.F.C. The V.F. presented to the H.O. is, in this case, the T.V. monitor image as seen by a body fixed T.V. camera. It is assumed that image rolling is prevented either by roll stabilization of the camera, the image or the complete vehicle. This assumption is based on current experience that image rolling can be detrimental in the control of R.P.V.'s.

If sideslip is neglected, the direction of motion is identical with the vehicle axis and line of sight of the camera, in other words, it is indicated by a fixed reference point on the T.V. monitor. R.P.V. control is thus accomplished by vehicle based reference points.

For more realistic vehicle dynamics, β is not zero and the velocity vector of the vehicle is no longer indicated by the fixed reference point. In this case, display of the velocity vector or future vehicle path may become essential in controlling the vehicle.

2.3 The Analytical Model for a Single Looking Distance

The single distance V.F.I. model of (4) is incorporated in an optimal control framework, derived from Kleinman et al[5, 10, 11]. It is based on the following assumptions:

1. The well-trained H.O., behaves in a near optimal manner, in accordance with a specified performance criterion and subject to his inherent limitations.
2. The H.O.'s perceptual process is modelled by linear optimal estimation theory.
3. Human limitations and sources of H.O. remnant are incorporated in the model.

Fig. 3 shows the block diagram with the following definitions:

$\underline{x}$: state vector of vehicle and disturbance
$\underline{\varepsilon}$: vector of perceived variables, linearly related to $\underline{x}$ through C
C : observation matrix C, defined by the V.F.I. model
u_c : control force commanded to the neuromuscular system, approximated by $1/(1+T_N s)$
u^* : actual H.O.'s control action
τ : H.O.'s time delay
v_e : observation noise component, accounting for uncertainty in the perception of ε
v_m : motor noise component, accounting for the fact that u^* is not precisely known to the H.O.

V_e, V_m : observation - and motor noise covariances, shown to be proportional to the variance of ε and u_c respectively, Levison et al.[4] (1969). Noise levels are defined as:

$$V_e\,[db] = 10\,\log_{10}\,[V_e/(\pi E\{\varepsilon^2\})]$$

$$V_m[db] = 10\,\log_{10}\,[V_m/(\pi E\{u_c^2\})]\ .$$

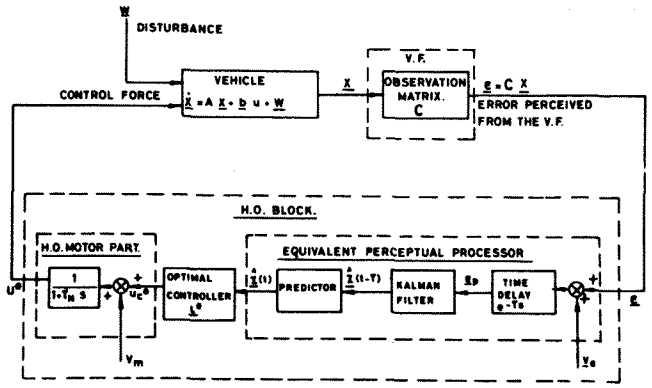

FIGURE 3. The Structure of the Optimal Control Model in Accordance with Ref. [5].

The H.O.'s control action involves:

1. Estimation of the state of the vehicle from the noisy, delayed observation, which action is assumed to be accomplished by Kalman filtering and optimal prediction.
2. Determination of the control force u. An optimal control $u = u^*$ is sought which minimizes, in the steady state, the cost function

$$J(u) = \lim_{T\to\infty} E\left\{\frac{1}{T}\int_0^T [\underline{x}^T Q\underline{x} + ru^2 + g\dot{u}^2]\ dt\right\} \qquad (6)$$

where Q is the weighting matrix of $\underline{x}$, and r and g the weighting coefficients of u and $\dot{u}$ respectively.

The solution of the estimation and control problem for single distance viewing is derived from Kleinman et al.[4,10,11] and given in the Appendix. The solutions yield the variances of η, ψ and u. These quantities, which are the characteristic measures of system performance, depend on the parameters D, r, τ, T_N and the observation rate noise covariance $V_{\dot{\varepsilon}}$. If these dependencies are sufficiently sensitive to variations in the above parameters, the analytical model can be useful as a research tool. A parametric study, designed to investigate these sensitivities has been performed. The results, shown in detail in[6], indicate that the model is sufficiently sensitive to enable meaningful comparisons with experimental results. An example, demonstrating this sensitivity to D and $V_{\dot{\varepsilon}}$ is shown in Fig. 4. The main effect of variations in the parameters are summarized as follows:

1. Increasing D results in a progresive increase of $E(\eta^2)$ and a monotonic decrease of $E(\psi^2)$ and $E(u^2)$. The reasons are that the estimate of η becomes poorer, and that of ψ becomes better. $E(u^2)$ decreases because the lead, given by (5) increases.
2. Increasing r results in a lower steering effort which is reflected into a higher η variance and a slightly lower ψ variance.
3. System performance is quite sensitive to $V_{\dot{\varepsilon}}$ in particular $E(\psi^2)$ at small D since then $\dot{\varepsilon}$ is comparatively large.

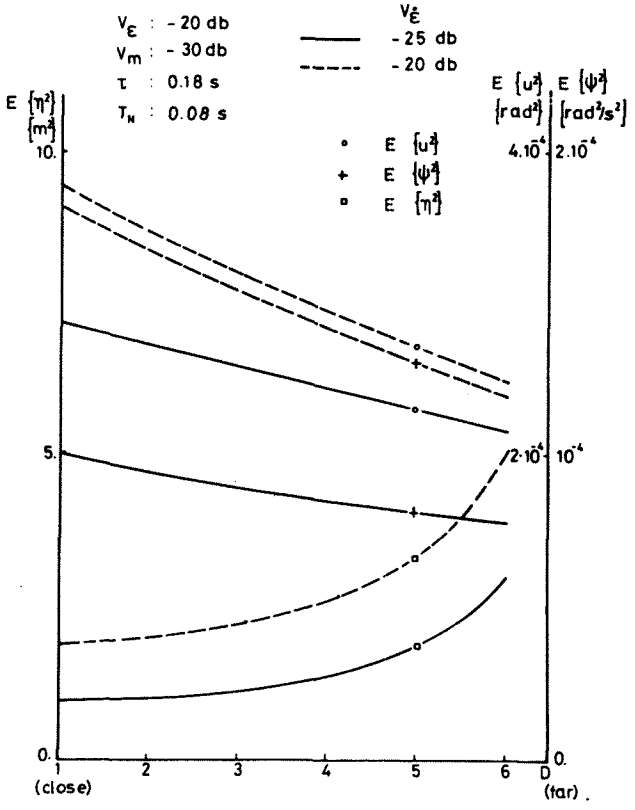

FIGURE 4. The Effect of Rate Observation Noise $V_{\dot{\varepsilon}}$ on $E(\psi^2)$, $E(\eta^2)$ and $E(u^2)$. (From Ref. [6]).

These trends and the sensitivities which were found in the parametric study, and discussed in greater detail in[6]) were considered sufficiently encouraging for an experimental validation of the analytical model.

2.4 Experimental Validation of the Single Distance Model

A five-dregree-of-freedom fixed-base simulator has been constructed which simulates a T.V. guided R.P.V. flight along a nominally straight reference trajectory. The degrees of freedom at present are: pitch motion (±30°), yaw motion (±30°), forward, lateral and vertical motion. H.O. commands are generated by an isomorphic high-precision strain gauge operated control manipulator. Vehicle motions computed by an E.A.I. 580 hybrid-analog computer are imparted to the appropriate pitch, yaw and translatory high-precision servo-systems, so that the projected scene, picked up by a T.V. camera, realistically simulates the relative vehicle motions. Atmospheric random disturbances are generated by a Hewlett-Packard HOI-3722-A noise generator. Input, state and output variables are recorded on magnetic tape by a Nova 2 digital computer and are further processed on an I.B.M. 360/370 computer.

The experiments concern a level, T.V. guided R.P.V. flight at a height h = 30 m, and a velocity V = 250 m/s. Vehicle dynamics are given by a double integrator (no sideslip). Figs. 5a - 5d show the V.F. as seen on a T.V. monitor. The

distance of the monitor from the operator is about 2.50 meters. The control task is to minimize the lateral deviation η from the reference trajectory HX.

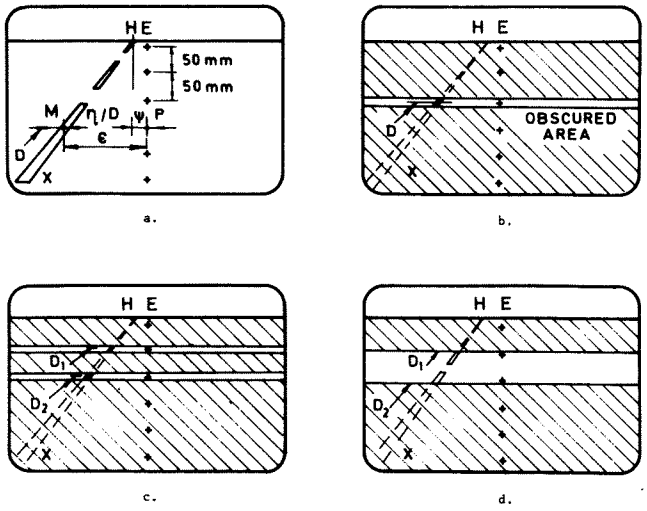

FIGURE 5. a. Complete V.F., Viewing Constrained to Single Distance.
b. Obscured V.F. Exposed at Single Distance.
c. Obscured V.F. Exposed at Two Distances.
d. Partial V.F. within a Span of Distances.

The starting point in the experimental program was to test the validity of the analytical model based on single distance V.F.I. according to (4). This model was found to be valid only if the subject's viewing was constrained by instructing him to look at a given distance D. However, when the subject's viewing was unconstrained, the experimental results were makedly different from those obtained by constrained viewing. This indicates a different extraction of the V.F.I. and a correspondingly different control strategy. It was of interest to study the type of V.F.I. model which best matches unconstrained viewing. For that purpose a V.F.I. model based on error detection at two looking distances was attempted.

2.4.1 Program Definition

The validation was carried out by the following tests:

I. Constrained single distance viewing experiments with the complete V.F. The complete V.F. is presented to the operator as shown in fig. 5a, displaying a dashed reference line. Texture points are not presented. The subject is instructed to eliminate the error ε. ε is indicated as the visual angle between a point M at distance D on the trajectory and a fixed point P on the monitor, which indicates the direction of motion. Six equidistant reference points were marked on the vertical center line of the T.V. monitor. In each test the subject was instructed to look at one point while completely disregarding the other points.

II. "Hovering" experiments with the V.F. exposed at one looking distance. All V.F.I. apart from ε and $\dot{\varepsilon}$ was eliminated so that the V.F.I. is strictly defined by (4). This was obtained by freezing the forward motion in the display (without altering the equations of motion) so that a "hovering" flight is simulated. The V.F. was obscured except for a very restricted zone at distance D, see fig. 5b. Thus V.F.C. was reduced to a basic single point tracking task. The purpose was to verify whether experimental and theoretical results match throughout a wide range of D, to determine unknown model parameters and to compare with results obtained by Kleinman et al.[5]

III. "Hovering" experiments with the V.F. exposed at two looking distances. Only two zones of the V.F. are shown at distances D_1 and D_2 under "hovering" conditions as in II, see fig. 5c. The control task is to eliminate the errors ε_1 and ε_2 corresponding to D_1 and D_2. The subject was not instructed with regards to his viewing and control strategy.

IV. V.F.C. experiments with unconstrained viewing and partial V.F. and forward motion. The complete span of the V.F. between the two distances D_1 and D_2 is shown as in fig. 5d. The subject has to eliminate the lateral error and is not instructed with regards to his viewing and control strategy.

2.4.2 Experimental Results

Tests I and II yielded practically the same results in all variables. A sample result for test II and for one subject is shown in fig. 6. More detailed results are given in[6]. In these tests, the variances of η, ψ and u were measured as function of D. The results were plotted and compared with a corresponding family of curves of the single distance analytical model, previously obtained by the parametric study of section 2.3. The curve closest to the corresponding experimental results establishes the best match from which model parameters are estimated. These curves, for one subject are shown in fig. 6 and indicate the following:

1. Theoretical and experimental results match closely over a broad range of D. This shows that the progressive increase of $E(\eta^2)$ and monotonic decrease of $E(\psi^2)$ and $E(u^2)$ as found in Sec. 2.3 and and shown in fig. 4 are indeed supported by the experiment.

2. The high sensitivity of the computed variances of η, ψ and u to variations in model parameters enabled the estimation of their experimental values with good confidence. The results agree in general with the tracking task results of Kleinman et al.[10 11] except for V_e and V_m for which smaller values were found.

Tests III and IV, concernced with two looking distances, yielded practically the same results for $E(\eta^2)$, $E(\psi^2)$ and $E(u^2)$. These are incorporated in fig. 6 and indicated by the arrows for the spans of viewing distances 4-6 and 5-6. The results indicate the following:

1. In all cases $E(\eta^2)$ is considerably lower than for the single looking distance model. $E(\psi^2)$ is only slightly smaller while $E(u^2)$ is slightly higher.

2. No point can be found on the curves of the single distance model which matches with the two-distance or free viewing experimental results.

These results indicate that the single distance analytical model does not adequately represent the

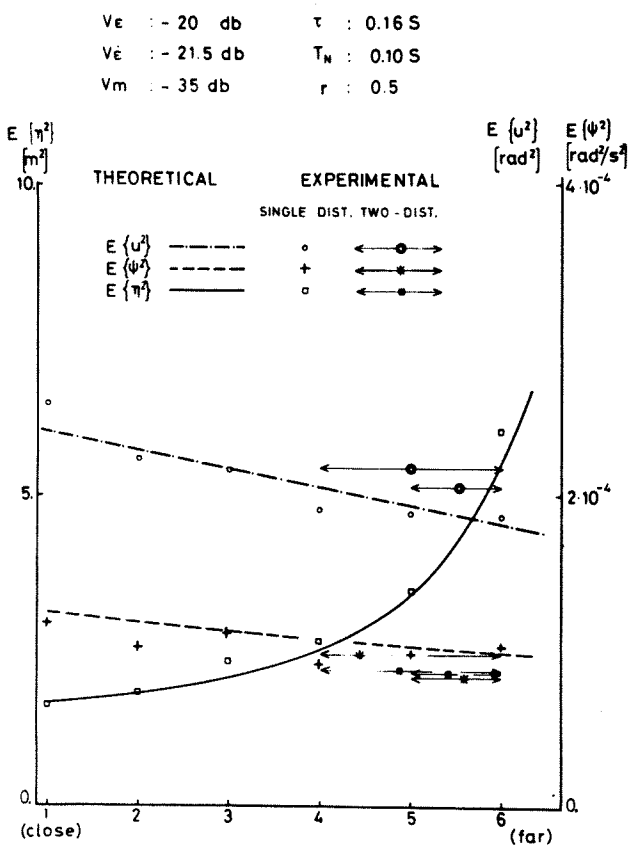

FIGURE 6. Comparison of Analytical and Experimental Performance for Single and Two-Distance Viewing (From Ref.[6]).

actual free viewing and control functions of the human operator. Consequently, the analytical model was extended for two distance viewing.

2.5 Analytical Model for Two-Distance Viewing

An analytical two-distance V.F.I. model is defined, in which both errors ε_1 and ε_2 , corresponding to D_1, D_2, as well as the error rates $\dot{\varepsilon}_1$ and $\dot{\varepsilon}_2$ are the perceived variables.

$\varepsilon_1+\varepsilon_2$ represents the error of a midpoint and $\varepsilon_1-\varepsilon_2$ the inclination of line HX, fig. 6c. The utilization of $\varepsilon_1-\varepsilon_2$ in addition to $\varepsilon_1+\varepsilon_2$ is the manifestation of the additional V.F.I. provided by the two distance model and is formulated in the following cost function:

$$J(u) = E\{(\varepsilon_1+\varepsilon_2)^2 + c(\varepsilon_1-\varepsilon_2)^2 + ru^2 + q\dot{u}^2\} \quad (7)$$

where the weighting coefficient c determines the control strategy:

1. $c = 0$ all weighting is given to $(\varepsilon_1+\varepsilon_2)^2$ and the two-distance task reduces to a single distance tracking task of the midpoint.
2. $c = 1$ equal weighting is given to ε_1^2 and ε_2^2.
3. $c >> 1$ large weighting is given to $(\varepsilon_1-\varepsilon_2)^2$ in other words, to η.

The correspondingly modified observation matrix C and weighting matrix P are defined in the Appendix in Eqs. (40) and (46).

In section 2.4 observation - and rate observation noise levels were set to about -20 db for hovering tests with the V.F. exposed at a single distance. In the development of the two-distance analytical model a suitable range of noise levels has to be assumed. At best the -20 db noise level of the single distance model is maintained. On the other hand, following Levison's concept of task interference[15], the noise level at each point may increase by a factor of 2 i.e., -17 db. Consequently in the parametric study of the two distance model V_ε is scanned between -17 and -20 db. Results of such a parametric study are shown in Fig. 7. The family of curves shows the computed values of $E(\eta^2)$, $E(\psi^2)$ and $E(u^2)$ as a function of the weighting coefficient c with V_ε as a parameter and for a span of looking distances corresponding to points 4-6. As expected, increasing c, i.e., stronger weight on η, decreases $E(\eta^2)$ at the expense of higher values of $E(\psi^2)$ and $E(u^2)$. In Fig. 7, a sample of experimental results for one subject is shown for the two-distance hovering task with the span of distances corresponding to points 4-6. The following observations apply:

1. V_ε [db] = -17 yields a close match for η and u at c = 15 whereas $E(\psi^2)$ found experimentally, is below the theoretical curve. This indicates that V_ε [db] = = -17 is a slightly too high assumption.

2. For V_ε [db] = -18, c = 7.5 η and ψ match whereas $E(u^2)$ found experimentally is above the theoretical curve, which means that V_ε [db] is slightly higher than -18.

3. This shows that V_ε [db] in reality must be between -17 and -18 and c between 7.5 and 15.

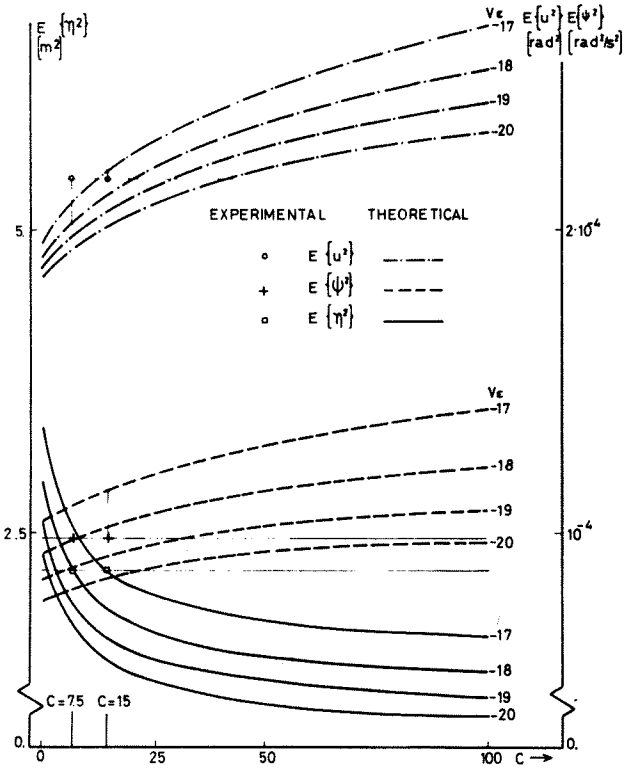

FIGURE 7. Matching of Computed and Experimental Performance for Hovering with the V.F. Exposed at Distances 4 and 6. (From Ref. [6]).

Similar results were obtained with other subjects tested under the same conditions. For the distance span 5-6 again, a very good match between theory and experiment was obtained. As predicted by the analytical model the appropriate value of c was considerably higher (more weighting on η) and was found to be $c \sim 25$.

2.6 Conclusions and Further Work

1. The results demonstrate the power of man-machine modeling in a control theoretical framework and the possibility of developing a sophisticated analytical overall system model from which performances and sensitivity to variations in parameters can be predicted.

2. A remarkably good match is found between the theoretical and experimental results. The wide range of parameters for which this match holds, supports the confidence in the validity of the analytical model and enables the estimation of unknown H.O. parameters within narrow limits.

3. The two-distance V.F.I. model is a valid representation of the V.F.C. task with unconstrained viewing.

The results which pertain to a simplified model of vehicle dynamics without sideslip, encouraged further studies for complete vehicle dynamics including sideslip.[16] For these realistic vehicle models, more state variable components are generally required for the effective control of the vehicle. Frequently, these are provided by the direction of the streamers, which have been disregarded in the present paper. The information provided by streamers can be re-established artificially by display aids which are superimposed on the visual scene, e.g., a section of the predicted future path, which as mentioned in Sec. 2.2., is equivalent to the central streamer. These further studies, carried out in a control theoretic framework, and extensively validated by experiments, clearly indicate the relation between the effectivity of several types of displays such as fixed reticle, velocity vector, predicted future path and the dynamics of the controlled vehicle and the disturbance bandwidth.

3. A Model for Manual Control with Kinesthetic Information from the Manipulator

3.1 Background

Conventional manipulators are essentially passive linear transducers which translate manual commands into electrical input signals. In accordance with control theoretic man-vehicle models, e.g., Mc Ruer et al[1] (1967), Kleinman et al[5] (1970), the generation of these manual commands requires state estimation and optimum weighting which are executed by the functions of visual perception and cerebral data processing of the central nervous system. This explains the considerable workload generally experienced in the manual control of dynamical systems. Several studies in recent years attempted to reveal whether, and to what extent, isotonic, isomorphic, isometric, inertia loaded, or other passive manipulators affect tracking and regulation performance[17,18].

Since the muscle spindles and Golgi tendons in the manual neuromotor system provide position velocity and force measurements[3], different combinations of neuromotor loop closures should be involved in the operation of various types of passive manipulators. Recent laboratory open-loop tracking tests[19] have indeed revealed significantly different motor noise levels indicating such differences. They become, however, insignificant in closed loop tracking tasks as a result of the overriding supervisory visual loop closure. The dominant factors which determine performance and stress, remain plant dynamics and system inputs, since the operations of state estimation and optimal weighting[5] are essentially the same with all types of passive manipulators. An interesting attempt to overcome this shortcoming of passive manipulators is due to Herzog[20] (1969), who studied the effect of a "matched manipulator." It ideally consists of a plant inverse operator at the input of the controlled plant. Thus, the human operator is always presented with a zero order system. Torque loading proportional to the plant input was applied to the manipulator so that an illusion of "natural feel" was provided. Significant improvement in tracking accuracies was reported[20] even when the manipulator match was not perfect. Two major shortcomings in this concept are apparent: 1) Inadequacy for systems with large parameter variations. 2) Absence of response to external disturbances. Thus no advantage over passive manipulators exists in this important respect. Other investigations with similar techniques for the control of unstable systems were reported by Noggle[21] (1969) and more recently a tactile display of angle of attack was reported by Gilson et al[22] (1974), in particular when much attention was required in the visual channel.

In order to establish the basis of a control theoretic framework for manual control system and to provide a better understanding for the variables involved in different types of manipulators, the basic and most familiar systems are described qualitatively in the following section.

3.2 Basic Manipulator Models

Figs. 8 and 9 schematically describe the interconnections of basic manipulators with the man-machine system, and their corresponding kinesthetic feedback paths. The diagrams suggest that the commanded scalar control u_c consists of a contribution u_c^V from the central nervous system which comprises visual perception and cerebral processing and a contribution u_c^N from the manual neuromuscular center associated with the cerebellum. In the sequel it is shown that the type of manipulator determines whether the visual-cerebral or the manual neuromotor center carries the main burden in the control task. A desired goal is clearly to achieve the latter. A control theoretic approach suggests that in either case, estimates $\hat{\underline{x}}$ and $\hat{u}$ of the system state $\underline{x}$ and control force u are available so that an optimal weighting matrix $\underline{l}$ can be set in accordance with a suitable performance criterion. Fig. 8 represents the situation of the direct handling of an object (natural feel). In this case the system output y equals the manual deflection c. T_i, the torque exerted by the muscle output equals the reaction torque T_0 and is identical to the plant control input u. Various muscle sensors (mostly spindles G_{sp}) measure position $x = x_1$, velocity $\dot{x} = x_2$ from $\dot{y}$ [1,3]. The Golgi tendons [1] G_k measure, T_i or u. These signals, corrupted by their corresponding measurements noises V_p and V_k yield the estimates $\hat{\underline{x}}_N$ and $\hat{u}_N$. Thus, the optimal

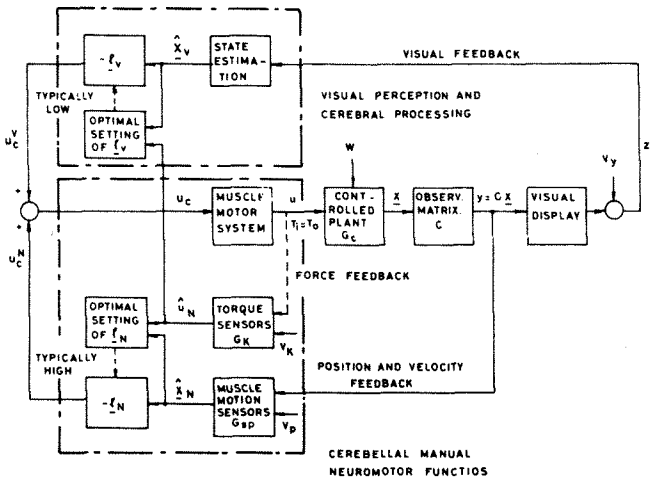

FIGURE 8. Schematic Description of the Manual control System in Direct Handling of Objects. (From Ref.[7]).

setting of l_N is possible and $u_c^N = -l_N \hat{x}_N$ is a substantial contribution to the control signal u_c. Consequently the contribution of the visual center $u_c^v = -l_v \hat{x}_v$ will be comparatively small. This explains the small workload involved in direct handling of objects and the relative ease of manual operations in darkness or with closed eyes. Only in operations which require expreme precision (as the threading of a needle) the main burden is on the visual channel since a large l_v is required to suppress the effect of V_k and V_p. This is possible, since V_y is very small by comparison.

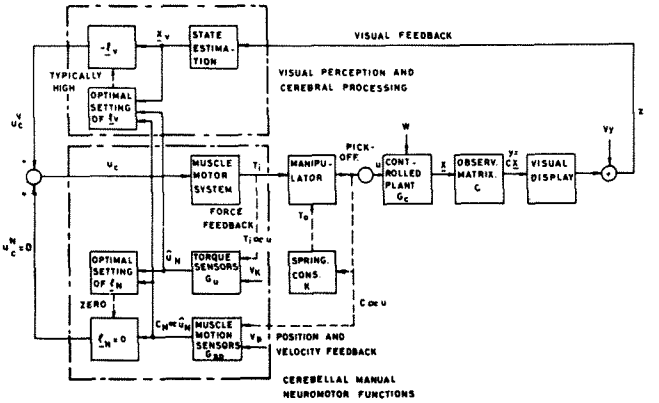

FIGURE 9. Schematic Description of the Manual Control System with a Passive Isomorphic Manipulator (From Ref.[7]).

Figure 9 describes the man-machine system with a conventional isomorphic manipulator. The kinesthetic information path is now disconnected from the plant output y. c, the manipulator deflection, is proportional to u. Since $T_0 = T_i = ku$ (k - spring constant), G_k and G_p both provide measures of u only. Since $\hat{x}_N$ is not present, the setting of l_N must be zero so that $u_c^N = 0$. Consequently, the central nervous system must take the entire control task load and the optimal setting of l_v is consequently high. The lack of kinesthetic information from the system output, thus explains the considerable workload which prevails with all types of passive manipulators: Isotonic (k=0), isomorphic ($k\neq 0$) and isometric ($k=\infty$). Only in the special case of a zero order plant, $y \propto c$. Thus that G_{sp} provides information proportional to $\hat{x}$ so that the setting of l_N can be high. This explains the small workload experienced in the control of zero order systems.

In the following section it is shown how complete kinesthetic input and output information can be provided and that the method involved can be implemented for a large variety of stable and unstable plants which may undergo large parameter variations.

3.3 Realization of Manipulator System with Complete Kinesthetic Information

Let $G_c(s)$ denote the plant dynamics. It is incorporated in the feedback path of a high gain amplifier K as shown in Fig. 10. N_1 and N_2 are compensation networks to ensure stability of the corresponding feedback loops. The plant input u is amplified by the power amplifier A driving the torque motor which is mechanically linked to the manipulator and the pick-off. Since $G_c(s)\ U(s) = Y(s)$ and $[Y_c(s) - Y(s)]KN_1(s) = U(s)$, it follows that:

$$\frac{Y(s)}{Y_c(s)} = \frac{K}{K + \dfrac{1}{N_1(s)G_c(s)}} \tag{8}$$

If it is possible to maintain the condition

$$K >> 1/N_1(s)G_c(s) \tag{9}$$

up to the frequency of $\omega \approx 20$ rad/sec, which is the effective bandwidth in manual control, then from (1) one has:

$$Y(s) \simeq Y_c(s) \tag{10}$$

Since $y_c \propto c$ (Fig. 10), it follows that the kinesthetic feedback path from c is equivalent to that from y in Fig. 8. Since $N_2(s)$ is in practice a wide band network, it follows that $T_0 \propto u$ in the relevant frequency band, and it is equivalent to the direct reaction torque T_0 in Fig. 8. In view of (9), equality (10) is insensitive to wide parameter variations in $G_c(s)$ and if $N_1(s)$ is suitably designed, (10) holds for an unstable $G_c(s)$ as well.

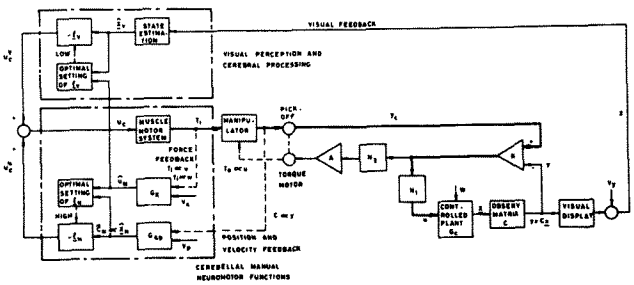

FIGURE 10. Realization of manipulator with complete kinesthetic information (From Ref.[7]).

It is easily verified that the reaction to the external disturbances $W(s)$ is satisfactorily provided by the system shown in Fig. 10.

In view of (9) and since $N_1(s) \approx 1$ in the effective frequency band, it is easily shown that:

$$Y(s) \approx Y_c(s) - \frac{W(s)}{K} \tag{11}$$

Thus, due to the large gain K, if $y_c = 0$, the response to the disturbance is effectively eliminated. The torque required to maintain $Y_c(s) \equiv 0$ is derived from $U(s)$ which is readily shown to be:

$$U(s) = KN_1(s) \frac{G_c(s)}{1+KN_1(s)G_c(s)} W(s) \approx W(s) \qquad (12)$$

Thus,

$$T_i(s) = U(s)AH \approx W(s)AH \qquad (13)$$

The value of A must be so adjusted that for a typical disturbance level of $W(s)$, $T_i(s)$ should not cause muscular fatigue.

From the foregoing it follows that the system shown in Fig. 10 provides complete kinesthetic information in equivalence to Fig. 8. With the proper design of $N_1(s)$ and $N_2(s)$ it can fulfil all the requirements regarding: 1) Wide variations of plant parameters. 2) Unstable systems. 3) External disturbances.

The actual design of the manipulator, using a brushless torque motor with a maximum torque of 12 Kg-cm is described in detail in [7]. The initial design of $N_1(s)$ and $N_2(s)$ was carried out for $G_c(s) = 1/s^2$. The detailed design confirms that the closed loop poles are either compensated by neighboring zeros or are outside the 20 rad/sec bandwidth. The required proportionality $c \propto y$ is effectively implemented. On replacing $G_c(s)$ by $1/s$, $1/s(s-1)$, $1/(s^2+0.66s+10)$ while retaining the same values for K, $N_1(s)$ and $N_2(s)$ as for $G_c(s) = 1/s^2$, it was found that the closed loop pole locations vary only slightly so that $c \propto y$ is guaranteed. It should be noted that though $c \propto y$ for different plants $G_c(s)$, large differences exist in the corresponding reaction torques T_0. For a given command output $Y_c(s)$, and since $Y(s) \approx Y_c(s)$, T_0 is given by

$$T_0(s) \simeq \frac{Y_c(s)}{G_c(s)} AH = uAH \qquad (14)$$

This kinesthetic display of u, characteristic of each G_c, in association with the output y_c enables the human operator to identify G_c by means of the cerebellal manual neuromotor functions (Fig. 10), and thus to execute optimal or near optimal control inputs. This is demonstrated in the next section.

3.4 Optimal Manual Fixed Set-Point Regulation

The objective is to eliminate an initial deflection y_0 subject to constraints on the control effort u. The controlled plant chosen is: $G_c(s) = k/s^2$. It involves two state variables, x and $\dot{x}$ which are compatible with the muscle sensors involved as explained in Sec. 2. A recorded sample of the time history of four such transient responses obtained in laboratory tests and the corresponding control inputs $u(t)$ are shown in Fig. 11. The results demonstrate the remarkable closeness between y and y_c and its excellent dynamic response. This, and the typical damped low order mode shape of the control time history $u(t)$, suggest that a linear control law is actually implemented by the human operator. This hypothesis was tested by a comparison with the optimal solution of the corresponding analytical model as follows:

The state space representation of $G_c(s)$ is:

$$\dot{\underline{x}}(t) = A\underline{x}(t) + Bu(t) \qquad (15)$$

The system matrix A is 2×2, $x_1 = x$ and $x_2 = \dot{x}$. The

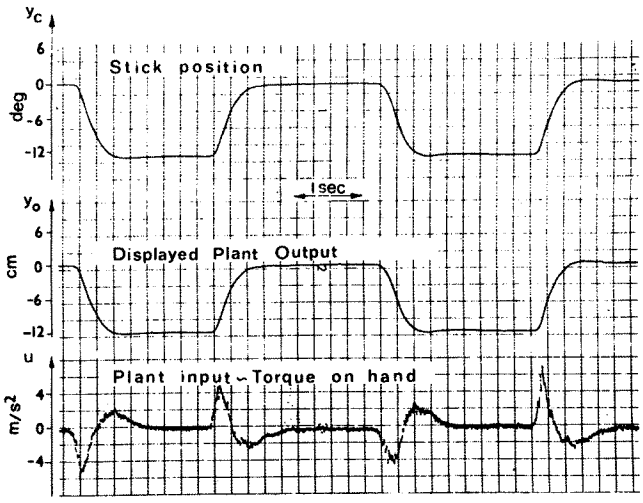

FIGURE 11. Time history of Transient Responses of a Fixed Set-Point Regulation Task for $G_c(s) = 1/s^2$. (From Ref. [7]).

controlled variable is

$$y(t) = C\underline{x}(t) \qquad (16)$$

$$C = (1,0) \quad ; \quad B = (0,k)^T \quad ; \quad A = \begin{pmatrix} 0 & 1 \\ 0 & 0 \end{pmatrix} \qquad (17)$$

The performance criterion which is assumed to underly the control policy is the minimization of:

$$J = \int_0^\infty [y^2(t) + \rho u^2(t)]\, dt \qquad (18)$$

$\rho \geq 0$ is the weight on the control effort.

In accordance with Fig. 8, the observed variable is:

$$z(t) = C\underline{x}(t) + V_y(t) \qquad (19)$$

where $V_y(t)$ represents white observation noise.

Let $\hat{\underline{x}} = (\hat{x}_1, \hat{x}_2)^T$ be the reconstructed state vector provided by a full state observer. The optimal control law is then given by:

$$u(t) = -\underline{l}\, \hat{\underline{x}}(t) \qquad (20)$$

where $\underline{l} = (1/\rho)\, B^T P$ and P is the solution of the 2×2 Ricatti equation $C^TC - PBB^TP + A^TP + PA = 0$. The result is:

$$\underline{l} = \left(\frac{1}{\sqrt{\rho}}, \quad \frac{2}{\sqrt{\rho}\, k} \right) \qquad (21)$$

The full state observer is of the form:

$$\dot{\hat{\underline{x}}}(t) = A\hat{\underline{x}}(t) + Bu(t) + K[y(t) - C\hat{\underline{x}}(t)] \qquad (22)$$

where $y(t) = C\underline{x}(t)$, and $K = (k_1, k_2)^T$.

Defining $\underline{e}(t) \triangleq \underline{x}(t) - \hat{\underline{x}}(t)$, the resulting augmented differential equation interconnecting $\underline{x}(t)$ and $\hat{\underline{x}}(t)$ for the closed loop system[23] is given by

$$\begin{bmatrix} \dot{\underline{x}}(t) \\ \dot{\underline{e}}(t) \end{bmatrix} = \begin{bmatrix} A-B\underline{l} & -B\underline{l} \\ 0 & A-KC \end{bmatrix} \begin{bmatrix} \underline{x}(t) \\ \underline{e}(t) \end{bmatrix} \qquad (23)$$

The characteristic values can be shown to be those of $A-B\underline{l}$ (regulator poles) and those of $A-KC$ (observer poles). For the example under consideration, the characteristic equation of $(A-B\underline{l})$ is $s^2 + (2k/\sqrt{\rho})^{1/2}s + k/\sqrt{\rho}$ so that the regulator poles are completely determined by the ratio $k/\sqrt{\rho}$. The

characteristic equation of the observer is $s^2 + k_1 s + k_2$. We assume that its damping factor is $\xi = 0.7$ so that $k_1 = \sqrt{2k_2}$. For the fixed set point regulation task considered here, the initial conditions for $(\underline{x},\underline{e})^T$ in (23) are assumed to be: $(\underline{x}_0,\underline{e}_0)^T = (x_1(0),0,e_1(0),e_2(0))^T = (x_1(0),0,x_1(0),0)^T$. With these assumptions, a numerical solution of (23) yields $\hat{\underline{x}}(t)$ from $\underline{x}(t)-\underline{e}(t)$ and $u(t)$ from (20) and (21). In this solution, k is known. ρ and k_1 are adjusted until a close fit to an ensemble average of $u(t)$ in Fig. 11 is obtained. The best values, with $k = 1$, were found to be: $\rho = 1/25$ and $k_1 = 12$. The result of this fit, shown in Fig. 12 supports the hypothesis of a linear control policy subject to a quadratic performance criterion of the type given in (18). The fixed set point regulating task was also performed for smaller values of manipulator stiffness S. The resulting control time histories of $u(t)$ were of similar form in Fig. 11. They had larger amplitudes and shorter durations. This is to be expected since smaller torques are involved and smaller values of ρ can be afforded by the human operator. It follows therefore that with complete kinesthetic information, the human operator controlling $G_c(s) = k/s^2$ resembles a linear optimal regulator, subject to a quadratic performance criterion with an energy constraint (18). It can be expected that for a different type of a second order plant $G_c(s)$, the solution would be of the same form but with a different setting of $\underline{l}$ and, therefore, ρ.

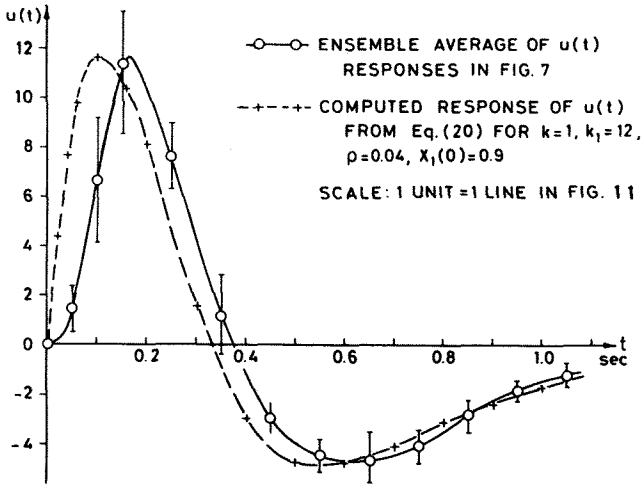

FIGURE 12. Comparison of Computed Optimal Response of $u(t)$ with Ensemble Averaged Measured Responses in Fig. 11 (From Ref. [7]).

It is also interesting to compare the transfer function relating $U(s)$ to $Y(s)$

$$H_c(s) = \frac{k}{s^2 + (2k/\sqrt{\rho})^{1/2} s + k/\sqrt{\rho}} \qquad (24)$$

which is the regulator block in (23), with the neuromuscular limb - manipulator model according to Mc Ruer et al[3]. From this model it follows that the transfer function for a purely intertially loaded manipulator (equivalent to our example $G_c(s) = k/s^2$), $U_c(s)$ is related to $C(s)$, (Fig. 10) by the approximate expression

$$\frac{C(s)}{U_c(s)} = \frac{C_f/M}{s^2 + (B_m/M)s + K_{sp}C_f/M} \qquad (25)$$

where:

K_{sp} - Muscle spindle gain factor
C_f - $\partial P/\partial f$; P - Muscle Tension; f - Neuromotor firing rate
M - Combined limb-manipulator mass
B_m - $\partial P/\partial V$, muscle damping factor; V - limb velocity

Since $T_0 = AHu$ and since $U(s) = Y(s)s^2/k$, it follows that $T_0(s) = (AH/k)s^2Y(s)$. Thus, AH/k is equivalent to a mass M. Since $c \propto y$, it is justified to compare (25) to (24) since they have the same form. The corresponding coefficients are: $(2k/\sqrt{\rho})^{1/2} = B_m/M$ and $k/\sqrt{\rho} = K_{sp}C_f/M$. The parameters B_m and C_f can be varied widely by the operator[3]. Thus, for different values of M, the neuromuscular system has sufficient freedom to adjust the optimal parameter values dictated by (24). This is apparently achieved by the independent control of B_m and C_f.

3.5 Performance in Tracking and Regulating Tasks

The optimal like performance achieved, with the kinesthetic manipulator should also be reflected in the error and workload associated with tracking and regulating tasks under stochastic stationary conditions. These effects were experimentally determined as follows: All tests were carried out so that every type of $G_c(s)$ was tested both for the kinesthetic manipulator mode and the conventional isomorphic manipulator mode. In practice, in order to keep all other factors unchanged, the same manipulator was switched into the system in either the isomorphic or the kinesthetic mode.

In all tests the primary task was tracking and/or regulating $G_c(s)$ for a stationary random input or disturbance band limited to ~1 rad/sec. The control test was single axis and in the vertical plane.

In order to obtain a measure of workload, a secondary task method was developed and adopted in the evaluation. A general block diagram is given in Fig. 13. The method consists of reading out (to permit supervision) of two-digit random numbers displayed outside the foveal field of the primary task display. The random numbers change at an increasing rate $\lambda(t) = Bt$, where B is a constant. During the initial 20 seconds, the operator concentrates on the primary task only and the initial mean squared error $\overline{e_f^2}$ is determined. Thereafter the secondary task is activated. The operator has to control the primary task but simultaneously read out the random

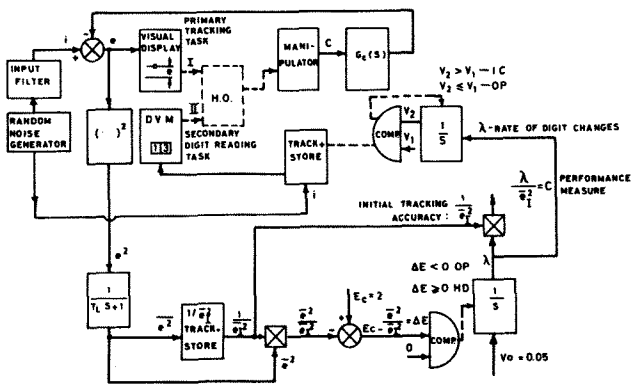

FIGURE 13. Schematic Diagram of the Evaluation System with a Secondary task Loading. (From Ref. [7]).

numbers the subsequent error variance $\overline{e^2}$ is normalized with respect to $\overline{e_f^2}$ as in Jex [24]. Due to the workload of the secondary task $\overline{e^2}/\overline{e_f^2}$ gradually increases. When some predetermined level E_c is reached, the system automatically stops at $\lambda = \lambda_c$. The performance measure was chosen as $C = \lambda_c/\overline{e_f^2}$. A comparatively easy task will have a small $\overline{e_f^2}$ and a large λ_c and vice versa. Thus, a large value of $C = \lambda_c/\overline{e_f^2}$ indicates a system with good accuracy and low workload. It easily verified that the method meets all three requirements listed above. In particular, the operator has no choice of "clever" strategies. For example, if he chooses initially to devote less attention to the primary task in order to reach a higher λ_c, his initial $\overline{e_f^2}$ will tend to be larger so that C tends to remain constant. The noise generator output i provides both the primary task input and the random numbers to the secondary task display. Preliminary tests of the evaluation method with several subjects demonstrated that the asymptotic well trained level of C is significantly and consistently different for different types of $G_c(s)$ like $1/s$, $1/s^2$, $1/s(s-1)$. The method was therefore adopted for the comparative evaluation of the kinesthetic manipulator. The tracking and regulation experiments, described in detail in [7], were carried out by a group of five students with no flying experience. They were selected from a larger group after undergoing preliminary screening tests of reaction time and tracking ability.

A set of results of tests with a random disturbance W and an uncorrelated random input i is shown in Fig. 14. The results are for three subjects with ten tests each. The following conclusions can be drawn:

1. For the isomorphic manipulator the performance measure $C_2 = \lambda_c/\overline{e_f^2}$ is the more significantly lower

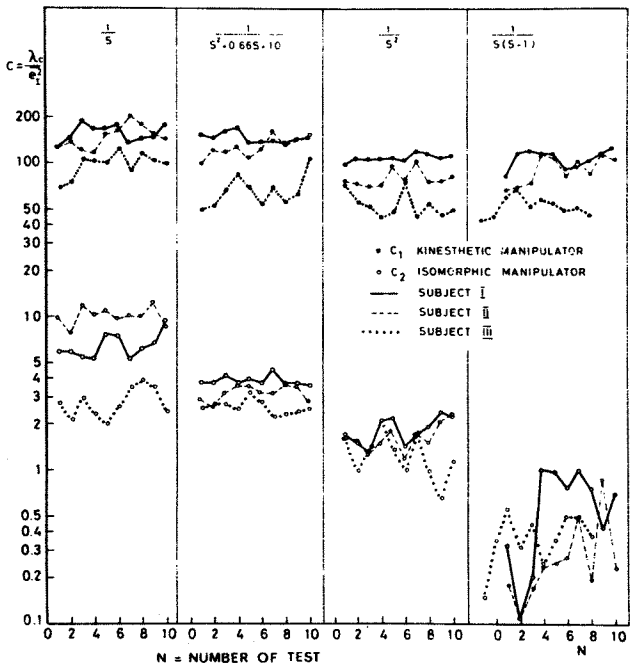

FIGURE 14. Results of Combined Tracking and Regulating Experiments (From Ref.[7]).

the harder the control task. This demonstrates the increasing workload associated with difficult control tasks due to the load on the visual channel and mental processing.

2. For the kinesthetic manipulator, $\lambda_c/\overline{e_f^2}$ is practically the same for all types of $G_c(s)$ and it is considerably higher. This demonstrates the unloading of the visual channel by the provision of complete kinesthetic information paths. It is significant that even an unstable system yields the same performance measure.

In all tests $\overline{e_f^2}$ with the kinesthetic manipulator was 3÷10 times smaller than with the isomorphic manipulator depending on the type of $G_c(s)$.

3. The considerable reduction in workload achieved by the kinesthetic manipulator confirms the assumption that the manual sensory organs as described in Sec. 3.2 are effectively involved to generate optimal like control commands at the proprioceptive level.

5. Discussion

The examples described in this paper demonstrate that the interfaces interconnecting the human operator with the controlled vehicle can be modelled in a meaningful manner so that a complete mathematical model of the man-machine system can be formulated and treated within the framework of modern control theory. In the first example, this interfacing takes the form of an observation matrix C, and in the second example it is manifested by the kinesthetic information T_i and y_c provided by the manipulator. In both examples, the close resemblance between theoretical and experimental results appears to provide good evidence for the optimality of the human operator in control and regulating tasks and that the approach of optimal control in man-machine research holds promise with regard to the theoretical development of this area and improved designs for man-machine interfaces both at the display and the control level.

6. Appendix
The Equations of the Optimal Control Model

6.1 Vehicle and Disturbance

The vehicle dynamics are given by:

$$\dot{\psi} = k\, u \tag{26}$$

$$\dot{\eta} = V\, \psi \tag{27}$$

The external disturbance is filtered zero mean Gaussian white noise w with convariance W. The noise filter is given by

$$\dot{u}_d = -a\, u_d + w \tag{28}$$

where u_d is the filter output and added to u. u_d is defined as an additional state component.

6.2 Optimal Controller

A control $u(t)$ is sought that minimizes in the steady state:

$$J(u) = E\{\varepsilon^2 + ru^2 + g\dot{u}^2\} \tag{29}$$

To include $\dot{u}$ an augmented state vector $\underline{\chi}(t)$ and an

alternative control $\mu(t)$ are defined:

$$\underline{\chi}(t) \triangleq \begin{bmatrix} \psi(t) \\ \eta(t) \\ u_d(t) \\ u(t) \end{bmatrix} \quad \text{and} \quad \mu(t) \triangleq \dot{u}(t) \tag{30}$$

The augmented state space equation becomes

$$\begin{bmatrix} \dot{\psi}(t) \\ \dot{\eta}(t) \\ \dot{u}_d(t) \\ \dot{u}(t) \end{bmatrix} = \begin{bmatrix} 0 & 0 & k & k \\ V & 0 & 0 & 0 \\ 0 & 0 & -a & 0 \\ 0 & 0 & 0 & 0 \end{bmatrix} \begin{bmatrix} \psi(t) \\ \eta(t) \\ u_d(t) \\ u(t) \end{bmatrix} + \begin{bmatrix} 0 \\ 0 \\ 0 \\ 1 \end{bmatrix} \mu(t) + \begin{bmatrix} 0 \\ 0 \\ w(t) \\ 0 \end{bmatrix} \tag{31}$$

or shortly written as

$$\dot{\underline{\chi}} = A_0 \underline{\chi}(t) + \underline{b}_0 \mu(t) + \underline{w}_0(t) \tag{32}$$

The optimal control solution is given by:

$$\mu(t) = -\underline{l}\underline{\chi}(t) \tag{33}$$

where $\underline{l} \triangleq [l_1\ l_2\ l_3\ l_4]$ is a row vector with the four optimal feedback gains and is given by:

$$\underline{l} = \frac{1}{g} \underline{b}_0^T K \tag{34}$$

where K is a 4×4 symmetric matrix and the solution of the four dimensional Riccati equation:

$$A_0^T K + K A_0 + Q - \frac{1}{g} K \underline{b}_0 \underline{b}_0^T K = \underline{0} \tag{35}$$

Q is the weighting matrix of $\underline{\chi}$ given by

$$Q = C^T P C \tag{36}$$

where C is the observation matrix and P the weighting matrix of perceived variables.

For single- and two-distance V.F.I., P is respectively given by:

$$P = \begin{bmatrix} 1 & 0 \\ 0 & 1 \end{bmatrix} \quad \text{and} \quad P = \begin{bmatrix} (1+c)/2 & 0 & (1-c)/2 & 0 \\ 0 & 0 & 0 & 0 \\ (1-c)/2 & 0 & (1+c)/2 & 0 \\ 0 & 0 & 0 & 0 \end{bmatrix} \tag{37}$$

Eq. (33) can be written as:

$$\mu(t) = \dot{u}(t) = -[l_1\psi(t) + l_2\eta(t) + l_3 u_d(t)] - l_4 u(t) \tag{38}$$

The commanded control u_c is defined as:

$$u_c = u + T_N \dot{u} \tag{39}$$

From combining eqs. (41), (38) it follows that:

$$u_c(t) = -[l_1\psi(t) + l_2\eta(t) + l_3 u_d(t)] T_N \tag{40}$$

and that T_N and l_4 are related by:

$$l_4 = \frac{1}{T_N} \tag{41}$$

6.3 The Estimation Process

The error ε and error rate $\dot{\varepsilon}$, perceived by the H.O. are corrupted with observation noise and delayed by τ seconds. The H.O. perceives $\underline{\varepsilon}_p$ given by:

$$\underline{\varepsilon}_p(t) = C\underline{\chi}(t-\tau) + \underline{v}_e(t-\tau) \tag{42}$$

and observation matrix C is as follows:

for single distance $\begin{bmatrix} 1 & 1/D & 0 & 0 \\ V/D & 0 & k & k \end{bmatrix}$

and for two-distance $\begin{bmatrix} 1 & 1/D_1 & 0 & 0 \\ V/D_1 & 0 & k & k \\ 1 & 1/D_2 & 0 & 0 \\ V/D_2 & 0 & k & k \end{bmatrix}$ (43)

$\underline{v}_e$ is the observation noise vector with noise covariance matrix V_e. With addition of the motor noise v_m (39) becomes:

$$u_c + v_m = u + T_N \dot{u} \tag{44}$$

and with (43) (31) is written as

$$\begin{bmatrix} \dot{\psi} \\ \dot{\eta} \\ \dot{u}_d \\ \dot{u} \end{bmatrix} = \begin{bmatrix} 0 & 0 & k & k \\ V & 0 & 0 & 0 \\ 0 & 0 & -a & 0 \\ 0 & 0 & 0 & \frac{1}{T_N} \end{bmatrix} \begin{bmatrix} \psi \\ \eta \\ u_d \\ u \end{bmatrix} + \begin{bmatrix} 0 \\ 0 \\ 0 \\ \frac{1}{T_N} \end{bmatrix} u_c + \begin{bmatrix} 0 \\ 0 \\ w \\ \frac{v_m}{T_N} \end{bmatrix} \tag{45}$$

or shortly written as

$$\dot{\underline{\chi}}(t) = A_1 \underline{\chi}(t) + \underline{b}_1 u_c(t) + \underline{w}_1(t) \tag{46}$$

The Kalman filter generates the delayed augmented state estimate $\hat{\underline{\chi}}(t-\tau)$ according to:

$$\dot{\hat{\underline{\chi}}}(t-\tau) = A_1 \hat{\underline{\chi}}(t-\tau) + \underline{b}_1 u_c(t-\tau) + \Sigma C^T V_e^{-1} [\underline{\varepsilon}_p(t) - C\hat{\underline{\chi}}(t-\tau)] \tag{47}$$

where Σ is the estimation error covariance matrix and the solution of:

$$A_1\Sigma + \Sigma A_1^T + W_1 - \Sigma C^T V_e^{-1} C \Sigma = \underline{0} \tag{48}$$

and W_1 the noise covariance matrix of $\underline{w}_1(t)$. The predictor generates the estimated present augmented state $\hat{\underline{\chi}}(t)$ from $\hat{\underline{\chi}}(t-\tau)$ by means of

$$\hat{\underline{\chi}}(t) = \underline{z}(t) + e^{A_1 \tau} [\hat{\underline{\chi}}(t-\tau) - \underline{z}(t-\tau)] \tag{49}$$

and

$$\dot{\underline{z}}(t) = A_1 \underline{z}(t) + \underline{b}_1 u_c(t) \tag{50}$$

A computer program computes the covariance matrices of $\underline{\chi}$ and $\underline{\varepsilon}$ as well as power spectra and H.O. transfer functions by means of closed form solutions, which are derived from Kleinman [25] (1970).

7. References

1. **McRuer, D.T., et al**, "Manual Control of Single-Loop Systems," *Journal of the Franklin Institute*, Vol. 283, No. 1, Jan. 1967, and No. 2, Feb. 1967.
2. **McRuer, D.T., et al**, *New Approaches to Human Pilot/Vehicle Dynamic Analysis*, Technical Report AFFDL-TR-67-150, Feb., 1968.
3. **McRuer, D.T., et al**, "A Neuromuscular Actuation System Model," *IEEE Transactions on Man Machine Systems*, Vol. MMS-9, No. 3, Sept.1968, pp. 61-71.
4. **Levison, W.H., Baron, S.**, and **Kleinman, D.L.**, "A Model for Human Controller Remnant," *IEEE Trans. on Man-Machine Systems*, Vol. MMS-10, No. 4, Dec. 1969.

5. **Kleinman, D.L., Baron, S.** and **Levison, W.H.**, "An Optimal Control Model of Human Response, Part I: Theory and Validation. Part II: Prediction of Human Performance in a Complex Task." *Automatica*, Vol. 6, 1970.

6. **Grunwald, A.**, and **Merhav, S.J.**, "Vehicular Control by Visual Field Cues - Analytical Model and Experimental Validation," to appear, *IEEE Trans. on Systems Man and Cybernetics*, Dec.1976.

7. **Merhav, S.J.**, and **Ben Ya'acov, O.**, "Control Augmentation and Workload Reduction by Kinesthetic Information from the Manipulator," to appear, *IEEE Trans. on Systems Man and Cybernetics*, Dec. 1976.

8. **Weir, D.H.**, and **McRuer, D.T.**, *A Theory for Driver Steering Control of Motor Vehicles*, Road User Characteristics, Highway Research Record No. 247, 1968.

9. **McRuer, D.T.**, and **Weir, D.H.**, "Theory of Manual Vehicular Control," *Ergonomics*, Vol. 12, No.4, pp. 599-633, 1969.

10. **Baron, S., Kleinman, D.L., Miller, D.C., Levison, W.H.**, and **Elkind, J.I.**, *Application of Optimal Control Theory to the Prediction of Human Performance in a Complex Task*, Wright-Patterson Air Force Base, AFFDL Rep. AFFDL-TR-69-81, 1970.

11. **Kleinman, D.L.**, and **Baron, S.**, *Manned Vehicle System Analysis by Means of Modern Control Theory*, NASA Contractor Rep., NASA CR-1753, June, 1971.

12. **Gibson, J.J.**, *The Perception of the Visual World*, Boston, Houghton Mifflin, 1950.

13. **Gordon, D.A.**, "Perceptual Basis of Vehicular Guidance," *Public Roads 34*, 53-68, 1966.

14. **Naish, J.M.**, "Control Information in Visual Flight," Douglas Paper No. 5921, *7th Annual Conference on Manual Control*, 1971.

15. **Levison, W.H., Elkind, J.I.**, and **Ward, J.L.** *Studies of Multivariable Manual Control Systems: A Model for Task Interference*, Nasa Contractor Rep., NASA CR-1746, May 1971.

16. **Grunwald, A.**, and **Merhav, S.J.**, *A Study of Display Augmentation in Visually Controlled Vehicles*, Department of Aeronautical Engineering, TAE Report No. 284, May, 1976.

17. **McRuer, D.T.**, and **Magdaleno, R.E.**, *Human Pilot Dynamics with Various Manipulators*, AFFDL-TR-66-138, 1966.

18. **Kraiss, K.F.**, "Can Proprioceptive cues unload the Human Operator," *6th An. Conference on Manual Control*, 1970.

19. **Ben Ya'acov, O.**, *Torque Feedback in Manual Control of Aircraft*, M.Sc. Thesis, Department of Aeronautical Engineering, Technion, May 1975.

20. **Herzog, H.J.**, *Proprioceptive Cues and Their Influence on Operator Performance in Manual Control*, NASA CR-1248, 1969.

21. **Noggle, P.L.**, *Manual Control of Unstable Vehicles Using Kinesthetic Cues*, MIT Report MV-69-4, 1969.

22. **Gilson, R.D., et al**, "Kinesthetic Tactual Information Presentation-Inflight Studies, *IEEE Trans. on SMC*, Vol. 4, pp. 531-536, 1974.

23. **Kwakernaak, H.**, and **Sivan, R.**, *Linear Optimal Control Systems*, Wiley, Interscience, 1972.

24. **Jex, H.R., et al**, "Development of the Dual Axis and Crosscoupled Critical Tasks, *8th Annual Conference on Manual Control*, May, 1972.

25. **Kleinman, D.L.**, "On an Iterative Technique for Riccati Equation Computations," *IEEE Trans. on Aut. Contr.*, Febr. 1968.